UV Photodissociation of Cyanoacetylene: A Combined Ion Imaging and Theoretical Investigation†

R. Silva,‡ W. K. Gichuhi,‡ V. V. Kislov,§ A. Landera,§ A. M. Mebel,*,§ and A. G. Suits*,‡

Department of Chemistry, Wayne State University, Detroit, Michigan 48202, and Department of Chemistry and Biochemistry, Florida International University, Miami, Florida 33199

Received: May 5, 2009; Revised Manuscript Received: June 11, 2009

The photodissociation of cyanoacetylene, one of the key minor constituents in Titan's atmosphere, was studied in a molecular beam under collisionless conditions using direct current slice ion imaging at 121.6, 193.3, and 243.2 nm. The experimental results were augmented by high-level theoretical calculations of stationary points on the ground-state and second excited singlet potential surfaces, and by statistical calculations of the dissociation rates and product branching on the ground-state surface. Results at 121.6 and 243.2 nm are nearly identical, suggesting that the 243.2 nm photodissociation is the result of a two-photon process. The translational energy distributions show only a modest fraction of the available energy in translation and are consistent with barrierless dissociation from the ground state. The results at 193.3 nm are quite distinct, showing up to half of the available energy in translation, implying dissociation with an exit barrier. The 193 nm result is ascribed to dissociation on the S_1 potential energy surface. The theoretical calculations show significant rates for H loss on the ground state at 193 nm and significant branching to CN + CCH at 157 nm and higher.

Introduction

The photodissociation of cyanoacetylene (CA), one of the key trace atmospheric constituents on Saturn's moon, Titan, is believed to be of central importance in the formation of the aerosol haze that dominates its atmosphere.[1−3] This has motivated many experimental and theoretical investigations of its photodissociation.[4−10] Halpern and co-workers have studied the photochemistry of CA and related compounds extensively, mostly in static cell experiments, using a variety of probe techniques but focusing mainly on the CN radical product.[6,7] Complex multiphoton processes were observed to give rise to a variety of radical products and emission from electronically excited CN and CCN. Clarke and Ferris used infrared absorption to investigate the UV photochemistry of CA by probing H−D exchange using a variety of deuterated reactants[4,11] with an interest in the role of CA photochemistry mediating ethane production on Titan. In a provocative study, Okabe and co-workers showed that UV irradiation of a cell containing a few torr CA promptly gave rise to an aerosol mist and a concomitant pressure decrease, suggesting rapid polymer formation.[10] They concluded that the primary dissociation process at 193 nm was H loss to form the radical CCCN with a quantum yield of 0.3. Radical reactions were then thought to lead to polymerization. The balance of the photoabsorption was believed to result in metastable HCCCN*, which could undergo subsequent reactions also contributing to polymer formation. Despite this large volume of previous work, direct laboratory investigation of photochemistry of CA under collisionless conditions in a supersonic molecular beam has not previously been undertaken.

The electronic spectrum of CA has been studied in absorption[10,12] and through excitation spectroscopy.[13] It consists of a weak band extending from 230 to 255 nm assigned to the vibronically induced $^1A'' \leftarrow {}^1\Sigma^+$ transition and a stronger, structured absorption from 190 to 225 nm assigned to a $^1\Delta \leftarrow {}^1\Sigma^+$ transition; in the vacuum ultraviolet there is a pair of broad, intense features at 146 and 141 nm as well as a series of intense Rydberg transitions beginning around 129 nm.[9,14]

Significant inconsistencies in the thermochemistry and bond dissociation energies have been reported over the years, with experimental D_0 values for H−CCCN reported as low as 117 kcal/mol[7,9] or 119.9 kcal/mol,[4,11] implying a dissociation threshold of 244 or 240 nm, respectively. Published theoretical values have consistently been much higher, ranging from 138 kcal/mol[15] to 130 kcal/mol,[8] giving instead dissociation thresholds from 208 to 219 nm. Resolving this discrepancy is important in understanding the role of CA photolysis in Titan's atmosphere, as the solar flux decreases significantly across this range. Experiment and theory agree that the H loss channel is the lowest dissociation pathway and that the onset of CCH + CN is significantly higher. The recent high-level theoretical study by Luo et al. is noteworthy in that they characterized the stationary points in the first excited singlet and triplet states as well as the ground state.[8] For the H loss channel, they found barrierless dissociation in the ground state but modest barriers on both S_1 and T_1, with the former correlating to electronically excited CCCN* ($^2\Pi$). These results will be considered further in the Discussion below.

In this paper we present direct current (dc) slice imaging results for photodissociation of CA under collisionless conditions at 121.6, 193.3, and 243.2 nm. These are combined with theoretical calculations of the stationary points on the ground- and excited-state surfaces (see Figure 1) and statistical calculations of the dissociation rates and product branching on S_0. The implications for the chemistry of carbon growth in Titan's atmosphere will also be considered.

† Part of the special section "Chemistry: Titan Atmosphere".

* To whom correspondence should be addressed. E-mail: mebela@fiu.edu; asuits@chem.wayne.edu.

‡ Wayne State University.

§ Florida International University.

10.1021/jp904183a CCC: $40.75 © 2009 American Chemical Society
Published on Web 07/06/2009

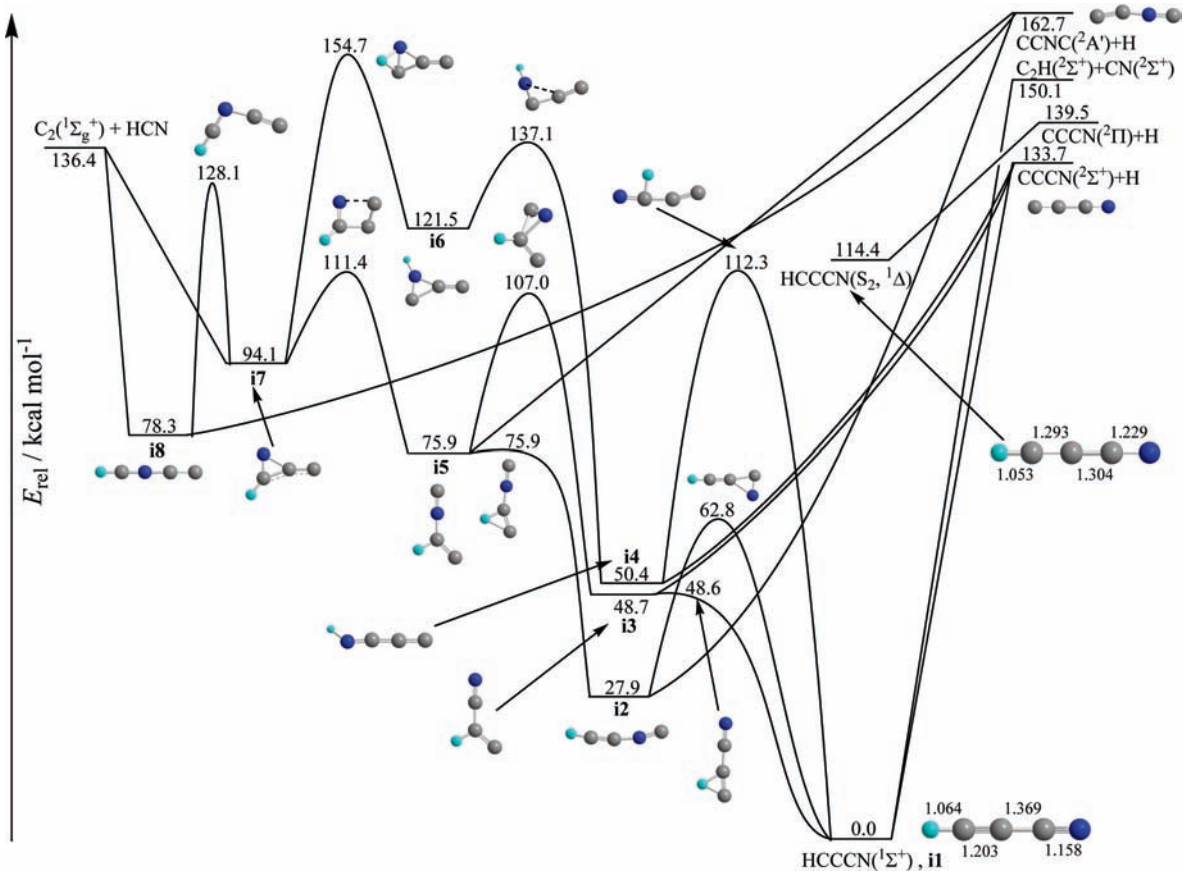

Figure 1. Stationary points and reaction pathways on the ground electronic state, and the S_2 minimum, for HCCCN calculated as described in the text.

Experimental Section

The experiment was carried out using a velocity map ion imaging[16,17] apparatus optimized for dc slice imaging.[18,19] A pulsed supersonic molecular beam containing ~2% cyanoacetylene seeded in argon was expanded from 1000 Torr via a piezoelectric pulsed valve into the source chamber held at $\sim 10^{-5}$ Torr. The laser and molecular beam delay was adjusted to access the earlier portion of the molecular beam pulse in order to eliminate the contribution from cyanoacetylene dimers/clusters. After dissociation by the 193 or 121 nm laser, the H photofragments were ionized by $(1 + 1')$ or Doppler-free $(2 + 1)$ REMPI schemes described below.[20] Next, the recoiling H^+ ion sphere, elongated along the flight direction, impacted onto a dual microchannel plate (MCP) array of 75 mm diameter coupled to a P-47 phosphor screen. Application of a narrow (40 ns) time gate at the detector was then used to sample the central section of the distribution. The resulting signal was recorded using a charge-coupled device (CCD) camera and a photomultiplier tube (PMT), in conjunction with the IMACQ megapixel acquisition program. This interface software was recently developed in our group,[15] enabling high-resolution real-time ion counting.

In the $(2 + 1)$ REMPI scheme for the 193 nm dissociation experiments, a 243 nm wavelength laser beam was produced by frequency doubling from a narrow-line-width (0.07 cm^{-1}) optical parametric oscillator (OPO) laser pumped at 355 nm, which was then split into two nearly identical beams using a 50−50 beam splitter. The beams were then sent into 1/4 wave retarders to produce circular polarized light in order to minimize the contribution from either laser alone.[20] The two counter-propagating laser beams, each with a power of ~1.8 mJ, were then focused with two 300 mm focusing lenses onto the molecular beam in the interaction region. The HC_3N was dissociated by an unpolarized 193 nm excimer laser beam, which propagated perpendicular to both the 243 probe beam and the molecular beam, and was focused by a 400 mm focal length lens. Product H atoms were then probed by a Doppler-free resonance-enhanced multiphoton ionization (DF-REMPI) scheme.

For the 243 nm dissociation experiments, an alternative approach, relying on the Autler−Townes effect, was used to give Doppler-free detection. In this approach, the fundamental 486 nm light was doubled and allowed to copropagate with the linearly polarized 243 nm light. The 486 nm light couples the 2s and 3d levels in atomic hydrogen, resulting in AC Stark broadening of the two-photon absorption to the 2s level. Conditions are readily found that broaden the line sufficiently to detect the full Doppler-broadened recoil distribution, but ionization on the line's center is suppressed,[21] as may be seen in the lower image in Figure 2 (below). This has little effect on the reconstructed distribution.

For the $(1 + 1')$ ionization, 121.6 nm light was generated by frequency tripling of 364.7 nm laser light, which was in turn produced by frequency doubling from a narrow bandwidth Sirah dye laser. The VUV light was produced in a cell containing 30% xenon gas, phase matched with argon at a total pressure of 900 Torr. The 364.7 nm beam was focused to the center of the VUV cell using a tight focusing quartz lens. The resultant Lyman-α light was then loosely focused to the center of the interaction region by a MgF_2 lens that also served as the exit window of the cell.

Cyanoacetylene was synthesized by a slight modification of the published procedure.[22,23] Briefly, 5.03 g of methyl propiolate

was reacted with 10 mL of ammonium hydroxide at −33 °C. The neat propiolate was added dropwise over a period of 10 min; the stirring bar was then removed and the water pumped off using a mechanical pump for about 8 h. The resulting yellow propiolamide crystals were then thoroughly mixed with 40 g of P_2O_5 and sand. The solid mixture of propiolamide, P_2O_5, and sand was then placed in a round-bottom flask and heated at 180 °C for about 1 h to yield cyanoacetylene, which was collected as a white solid at −78 °C.

Theoretical Methods

Molecular geometries and vibrational frequencies of HCCCN, various C_3NH local minima, and transition states were calculated at the hybrid density functional B3LYP/6-311G** level of theory[24,25] using the GAUSSIAN 98 package.[26] Relative energies of various species on the C_3NH ground-state potential energy surface were refined utilizing the coupled cluster CCSD(T) method as implemented in the MOLPRO program package[27] with extrapolation to the complete basis set (CBS) limit. To achieve this, we computed CCSD(T) total energies for each stationary point with Dunning's correlation-consistent cc-pVDZ, cc-pVTZ, cc-pVQZ, and cc-pV5Z basis sets[28] and projected them to CCSD(T)/CBS total energies by fitting the following equation,[29]

$$E_{tot}(x) = E_{tot}(\infty) + B\, e^{-Cx}$$

where x is the cardinal number of the basis set (2, 3, 4, and 5, respectively) and $E_{tot}(\infty)$ is the CCSD(T)/CBS total energy. For excited-state calculations, we employed an approach similar to that used by Luo et al.,[8] i.e., geometry optimization and vibrational frequency calculations at the complete active space self-consistent field (CASSCF) level with a (14,13) active space and the cc-pVTZ basis set, followed by refinement of single-point energies at the second-order multireference perturbation theory CASPT2(14,13)/cc-pVTZ level using the DALTON 2.0[30] and MOLPRO packages, respectively.

Results

Stationary points and dissociation asymptotes for the ground-state potential energy surface of CA are given in Figure 1 at the CCSD(T)/CBS level of theory. One can see that HCCCN **i1** can directly decompose to $CCCN(^2\Sigma^+) + H$ or $C_2H(^2\Sigma^+) + CN(^2\Sigma^+)$ by the cleavage of the C−H or the middle C−C bonds with an endothermicity of 133.7 or 150.1 kcal/mol, respectively, without exit barriers. Pathways to the other possible products, such as $CCNC(^2A') + H$ and $C_2(^1\Sigma_g^+) + HCN$ residing 162.7 and 136.4 kcal/mol above HCCCN, respectively, are more complex and will be discussed in detail elsewhere, in relation to the $C_2(^1\Sigma_g^+) + HCN$ reaction.[31] Here we only briefly mention that CCNC + H can be produced by C−H bond cleavages in HCCNC **i2**, CCHNC **i5**, and HCNCC **i8**, occurring without exit barriers. Since CCNC is computed to be 29 kcal/mol less stable than CCCN, the contribution of this product to the photodissociation of CA is expected to be insignificant. Energetically, the most favorable pathway leading to C_2 + HCN involves **i1** → **i2** rearrangement by flipping the CN group over, followed by a 1,2-H shift to **i5**, three-member ring closure to **i7**, and elimination of the C_2 fragment from the latter. **i7** can also ring-open to a peculiar HCNCC isomer **i8** and then lose C_2. Since the route to C_2 + HCN is rather complicated and includes entropically unfavorable H migrations and ring openings/closures, we expect that this product channel would play a relatively minor role.

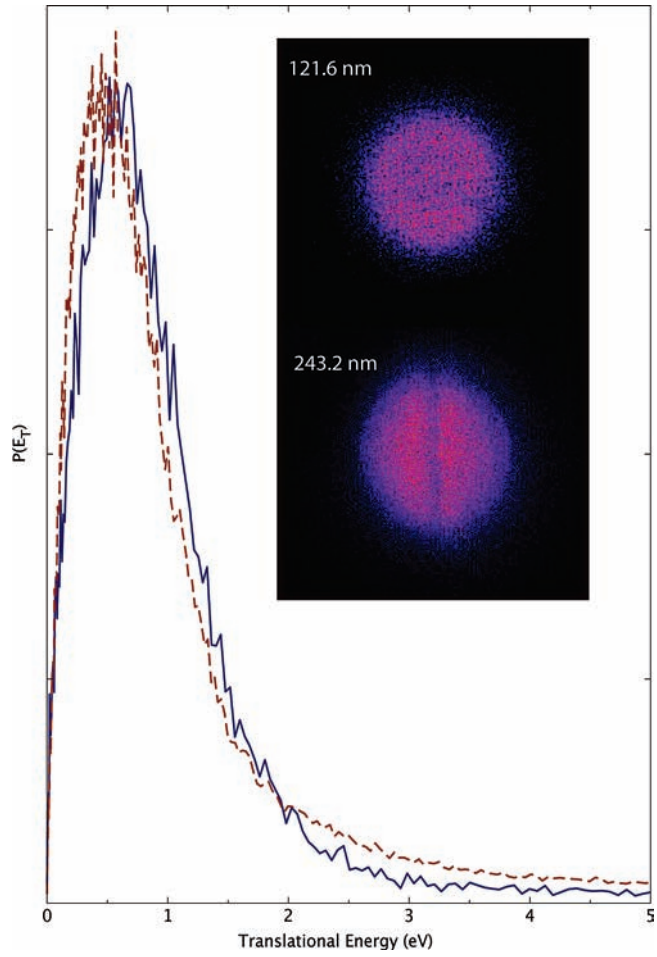

Figure 2. H^+ images at indicated wavelenth and associated translational energy distributions for cyanoacetylene dissociation at 121.6 nm (solid blue line) and 243.2 nm (red dashed line).

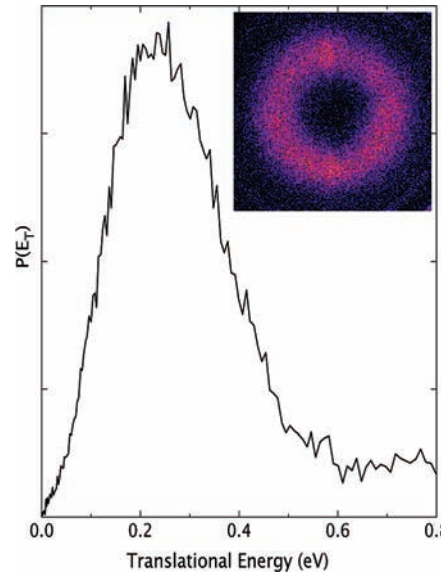

Figure 3. H^+ images and associated translational energy distribution for cyanoacetylene dissociation at 193.3 nm probed by Doppler-free REMPI at 243 nm.

Since dissociation of HCCCN on S_1 and T_1 surfaces was considered theoretically by Luo et al.,[8] here we focus our attention on the S_2 ($B\ ^1\Delta$) surface. The vertical excitation energy

TABLE 1: RRKM Calculated Rate Constants and Relative Yields for the CCCN + H and C_2H + CN Photodissociation Channels of Cyanoacetylene

photon wavelength, nm	212	193	157	121.6	2 × 212
available energy, kcal/mol	134.9	148.0	182.1	235.2	269.0
rate constant, s^{-1}					
HCCCN → C_2H + CN	0	4.25×10^7	1.44×10^{11}	2.20×10^{12}	5.70×10^{12}
HCCCN → CCCN + H	2.29×10^7	2.50×10^9	1.92×10^{11}	2.89×10^{12}	7.07×10^{12}
relative yield, %					
C_2H + CN	0	0	42.9	43.3	44.6
CCCN + H	100	100	57.1	56.7	55.4

from S_0 to S_2 computed in this work, 5.70 eV, is close to the result reported by Luo et al.[8] Geometry optimization for S_2 gives a stable structure, shown in Figure 1. One can see that, upon excitation to S_2, geometric changes involve elongation of the triple C≡C and C≡N bonds by ∼0.09 and ∼0.07 Å, respectively, accompanied by a shortening of the C—C single bond by 0.07 Å. In contrast to the S_1 and T_1 local minima, the optimized structure for S_2 maintains a linear $C_{\infty v}$ geometry. The calculated adiabatic excitation energy to the B $^1\Delta$ state is 4.96 eV (114.4 kcal/mol). Due to the computed change in geometry, vibrational modes that should be active in the $^1\Delta \leftarrow {}^1\Sigma^+$ absorption spectra include combinations of C≡N, C≡C, and C—C stretching, which are displaced and distorted in the excited state, with the corresponding vibrational frequencies changing from 2377, 2172, and 906 cm^{-1} in $^1\Sigma^+$ to 2075, 1465, and 938 cm^{-1}, respectively, in $^1\Delta$. These results support the assignment of the structured absorption band from 190 to 225 nm to the $^1\Delta \leftarrow {}^1\Sigma^+$ transition. A transition-state search for the H loss on the S_2 surface, carried out for the $^1A'$ component of $^1\Delta$ within C_s symmetry, showed that this process occurs without exit barrier and leads to the CCCN($^2\Pi$) + H products. Because of its degeneracy, the $^2\Pi$ state of the product correlates both with the S_1 ($^1A''$) and S_2 (the $^1A'$ component of $^1\Delta$ when symmetry is reduced to C_s) states of HCCCN. Thus, dissociation on the S_2 surface can also produce CCCN($^2\Pi$), but in contrast to the S_1 surface, no exit barrier was found here.

DC sliced ion images for H atom from dissociation/probe of CA at both 121.6 and 243.2 nm are shown in Figure 2, along with the translational energy distributions determined from the imaging data. The images show no angular anisotropy. The translational energy distributions are nearly identical, peaking at ∼0.5 eV and extending to 4−5 eV. The average translational energy release is 1.17 eV (243 nm) or 1.19 eV (121.6 nm), which is ∼27% of the available energy at Lyman-α. These are typical H atom loss distributions, similar to those we have seen from a range of hydrocarbon molecules, and they suggest dissociation on the ground electronic state following internal conversion. Despite the fact that the distributions peak away from zero energy, we believe they represent simple bond fission without a barrier. Statistical ground-state treatments are able to reproduce these distributions quite well, as has been shown by Ashfold and co-workers for ketene dissociation.[32] The similarity between the 243.2 nm result and that at Lyman-α strongly suggests that the former represents a two-photon absorption process. This is analogous to the situation we recently reported for diacetylene photodissociation. Although some of the earlier experimental work indicated dissociation thresholds for CA at wavelengths as long as 244 nm, this translational energy distribution at 243 nm is clearly not consistent with single photon dissociation near threshold.

The sliced ion image and associated translational energy distribution for 193 nm dissociation of CA are shown in Figure 3. This distribution is quite distinct from that at Lyman-α. It peaks at ∼0.2 eV and extends only to 0.5 eV, with an average of 0.30 eV. The theoretical results embodied in the energy diagram in Figure 1 give a dissociation energy of 133.7 kcal/mol, with an estimated uncertainty of perhaps 1 kcal/mol. This corresponds to a maximum available energy at 193.3 nm of 14.3 kcal/mol, or 0.62 eV. Our result at 193 nm thus shows roughly 50% of the available energy in translation. Alternatively, the excited-state S_1 surface correlates to electronically excited CCCN, roughly 0.2 eV higher in energy than the ground-state CCCN product (Figure 1). The maximum translational energy in that case would be 0.46 eV, which is very close to the observed limit. The triplet surface correlates to ground-state products and would give the higher tranlsational energy limit. As seen in Figure 1, direct dissociation on S_2 also correlates to the excited CCCN radical but occurs without a barrier.

Discussion

It is instructive to compare results for UV photoexcitation of CA to those for diacetylene. In both cases, H loss is the lowest energy dissociation channel,[33] but the threshold is higher than the absorption onset, and chemistry driven by "metastable" reaction has been invoked to account for reactive processes observed at energies below the dissociation threshold.[34−36] Furthermore, these dissociation thresholds were long thought to be much lower than the best current theory now suggests.[33] For CA in particular, the present theoretical value of 133.7 kcal/mol is not likely to be significantly in error. It is also well supported by the translational energy distribution in Figure 3. The previous experimental determinations of around 5.1 eV for the H−CCCN dissociation energy would imply a maximum translational energy limit of up to 1.3 eV for Figure 3. This is clearly not supported by the measurements.

The VUV dissociation result shown in Figure 2 is consistent with ground-state dissociation following internal conversion, although dissociation from higher excited states is not explicitly ruled out by the data. To understand the ground-state dissociation dynamics, RRKM calculations of the dissociation rates and product branching were performed just as we have recently reported for diacetylene.[33] The results are compiled in Table 1. Two significant differences are immediately apparent in these results compared to those reported for diacetylene. For CA, the dissociation rate at 193 nm is 2.50×10^9 s^{-1}; this is 50 times higher than that for diacetylene. This may account, in part, for our facile detection of the H loss channel in this case, while we were unable to obtain photodissociation results for diacetylene at 193 nm. The origin of this increased rate is the lower density of states for the dissociating molecule HCCCN vs HCCCCH. The second significant difference in these results relative to those found for diacetylene is in the branching to the H loss channel. For diacetylene, H loss dominated, 80% at 157 nm and 75% at Lyman-α. For CA, we see in Table 1 that branching to H loss quickly falls to 57% once the C_2H + CN channel is open and then remains roughly independent of excitation wavelength, decreasing only slightly. The higher yield of C_2H + CN from

cyanoacetylene vs $C_2H + C_2H$ from diacetylene can be understood if we compare the energy difference between $C_2H + CN$ and $CCCN + H$ (16.4 kcal/mol) and that between $C_2H + C_2H$ and $CCCCH + H$ (26.6 kcal/mol). Thus, the $C_2H + CN$ channel opens at a lower energy (150.1 kcal/mol), compared to 159.7 kcal/mol for $C_2H + C_2H$; as a result, the relative yield of the former nears its saturation earlier than that for the latter. Note also that possible minor production of $C_2 + HCN$ (up to ~10%) is not included here.

The image at 193 nm, shown in Figure 3, is quite intriguing. The fraction of available energy appearing in recoil is much higher than we usually see for H loss processes on the ground state. Although peaking away from zero energy in H loss from the ground state is commonly seen, usually it represents a relatively small fraction of the available energy.[32,33] A plausible explanation for the translational energy distribution in Figure 3 is dissociation from an excited state with an exit barrier on the order of 0.2 eV. As mentioned above, Luo et al. found barriers of ~0.06 eV for both S_1 and T_1 dissocation.[8] Although this is a bit low to account for the observed distribution, there is likely to be some significant associated uncertainty in the magnitude of the excited-state barriers. Furthermore, the S_1 dissociation correlates to electronically excited $^2\Pi$ CCCN product. The translational energy limit is very close to the theoretical prediction for this product. These observations lead us to suggest that 193 nm excitation likely gives rise to excited-state dissociation, yielding electronically excited CCCN.

Conclusions and Implications for Titan

We have observed photodissociation of cyanoacetylene under collisionless conditions at 193.3, 243.2, and 121.6 nm. The 243 nm result is assigned to a two-photon process, and its similarity to the Lyman-α result and the fact that both are isotropic, with relatively little energy in translation, lead to the likely assignment as ground-state processes. Theoretical calculations of the ground-state dissociation rates and branching show rapid H loss at 193.3 nm and branching to $HCC + CN$ above 40% at 157 nm and higher. The 193.3 nm result is in stark contrast, however. The sharply peaked translational energy distribution and large fraction of available energy in translation suggest excited-state dissociation, and the energetic limit leads to the likely assignment as S_1 dissociation.

At this point, the findings raise more questions than they answer for haze formation on Titan. Our results are consistent with the emerging theoretical consensus that the C−H bond in CA is much stronger than previously reported, making direct dissociation above 200 nm probably of limited significance. Furthermore, the results at 193 imply excited-state dissociation to electronically excited CCCN. This indicates that internal conversion is slower than that in diacetylene, for example. One must assume, however, that below the S_1 barrier, IC or ISC must eventually occur. The timing and wavelength dependence of these events will be important for understanding the possible role of metastable HCCCN in growth of hydrocarbons and nitriles in Titan's atmosphere.

Acknowledgment. This work was supported by the NSF under award number CHE-062784. We thank R. Kaiser for helpful discussions.

References and Notes

(1) Wilson, E. H.; Atreya, S. K. *Plan. Space Sci.* **2003**, *51*, 1017.
(2) Coustenis, A.; et al. *Icarus* **2007**, *189*, 35.
(3) Clarke, D. W.; Ferris, J. P. *Icarus* **1997**, *127*, 158.
(4) Clarke, D. W.; Ferris, J. P. J. *Geophys. Res.-Planets* **1996**, *101*, 7575.
(5) Kolos, R.; Zielinski, Z.; Grabowski, Z. R.; Mizerski, T. *Chem. Phys. Lett.* **1991**, *180*, 73.
(6) Halpern, J. B.; Petway, L.; Lu, R.; Jackson, W. M.; McCrary, V. R.; Nottingham, W. *J. Phys. Chem.* **1990**, *94*, 1869.
(7) Halpern, J. B.; Miller, G. E.; Okabe, H.; Nottingham, W. *J. Photochem. Photobiol.* **1988**, *42*, 63.
(8) Luo, C.; Du, W. N.; Duan, X. M.; Li, Z. S. *Appita J.* **2008**, *687*, 726.
(9) Okabe, H.; Dibeler, V. H. *J. Chem. Phys.* **1973**, *59*, 2430.
(10) Seki, K.; He, M. Q.; Liu, R. Z.; Okabe, H. *J. Phys. Chem.* **1996**, *100*, 5349.
(11) Clarke, D. W.; Ferris, J. P. *Icarus* **1995**, *115*, 119.
(12) Job, V. A.; W., K. G. *J. Mol. Spectrosc.* **1966**, *19*, 178.
(13) Titarchuk, T.; Halpern, J. B. *Chem. Phys. Lett.* **2000**, *323*, 305.
(14) Connors, R. E.; Roebber, J. L.; Weiss, K. *J. Chem. Phys.* **1974**, *60*, 5011.
(15) Francisco, J. S.; Richardson, S. L. *J. Chem. Phys.* **1994**, *101*, 7707.
(16) Chandler, D. W.; Houston, P. L. *J. Chem. Phys.* **1987**, *87*, 1445.
(17) Eppink, A. T. J. B.; Parker, D. H. *Rev. Sci. Instrum.* **1997**, *68*, 3477.
(18) Townsend, D.; Minitti, M. P.; Suits, A. G. *Rev. Sci. Instrum.* **2003**, *74*, 2530.
(19) Lee, S. K.; Silva, R.; Thamanna, S.; Vasyutinskii, O. S.; Suits, A. G. *J. Chem. Phys.* **2006**, 125.
(20) Riedel, J.; Dziarzhytski, S.; Kuczmann, A.; Renth, F.; Temps, F. *Chem. Phys. Lett.* **2005**, *414*, 473.
(21) Bowe, P.; O'Neill, R. W. O.; van der Burgt, P. J. M.; Slevin, J. A.; Racynski, A.; Zaremba, J.; Chwirot, S. J. *Phys. B* **1998**, *31*, 1003.
(22) Halter, R. J.; Fimmen, R. L.; McMahon, R. J.; Peebles, S. A.; Kuczkowski, R. L.; Stanton, J. F. *J. Am. Chem. Soc.* **2001**, *123*, 12353.
(23) Moreau, C. B.; Bongrand, J. C. *Ann. Chim. (Paris)* **1920**, *14*, 47.
(24) Lee, C. T.; Yang, W. T.; Parr, R. G. *Phys. Rev. B* **1988**, *37*, 785.
(25) Becke, A. D. *J. Chem. Phys.* **1993**, *98*, 5648.
(26) Frisch, M. J.; Trucks, G. W.; Schlegel, H. B.; Scuseria, G. E.; Robb, M. A.; Cheeseman, J. R.; Zakrzewski, V. G.; Montgomery, J. A., Jr.; Stratmann, R. E.; Burant, J. C.; Dapprich, S.; Millam, J. M.; Daniels, A. D.; Kudin, K. N.; Strain, M. C.; Farkas, O.; Tomasi, J.; Barone, V.; Cossi, M.; Cammi, R.; Mennucci, B.; Pomelli, C.; Adamo, C.; Clifford, S.; Ochterski, J.; Petersson, G. A.; Ayala, P. Y.; Cui, Q.; Morokuma, K.; Malick, D. K.; Rabuck, A. D.; Raghavachari, K.; Foresman, J. B.; Cioslowski, J.; Ortiz, J. V.; Stefanov, B. B.; Liu, G.; Liashenko, A.; Piskorz, P.; Komaromi, I.; Gomperts, R.; Martin, R. L.; Fox, D. J.; Keith, T.; Al-Laham, M. A.; Peng, C. Y.; Nanayakkara, A.; Gonzalez, C.; Challacombe, M.; Gill, P. M. W.; Johnson, B. G.; Chen, W.; Wong, M. W.; Andres, J. L.; Head-Gordon, M.; Replogle, E. S.; Pople, J. A. *Gaussian 98*, Revision A.9; Gaussian, Inc.: Pittsburgh, PA, 1998.
(27) Werner, H. J.; Knowles, P. J. *MOLPRO*, 2002.6 ed.; University of Birmingham: Birmingham, UK, 2003.
(28) Dunning, T. H. *J. Chem. Phys.* **1989**, *90*, 1007.
(29) Peterson, K. A.; Dunning, T. H. *J. Phys. Chem.* **1995**, *99*, 3898.
(30) Angeli, C.; et al. *DALTON, a molecular electronic structure program*, Release 2.0, 2005; http://www.kjemi.uio.no/software/dalton/dalton.html.
(31) Gu, X.; et al. *Astrophys. J.* **2009,** *699*, in press.
(32) Feltham, E. J.; Qadiri, R. H.; Cottrill, E. E. H.; Cook, P. A.; Cole, J. P.; Balint-Kurti, G. G.; Ashfold, M. N. R. *J. Chem. Phys.* **2003**, *119*, 6017.
(33) Silva, R.; Gichuhi, W. K.; Huang, C.; Doyle, M. B.; Kislov, V. V.; Mebel, A. M.; Suits, A. G. *Proc. Natl. Acad. Sci. U.S.A.* **2008**, *105*, 12713.
(34) Bandy, R. E.; Lakshminarayan, C.; Frost, R. K.; Zwier, T. S. *Science* **1992**, *258*, 1630.
(35) Frost, R. K.; Arrington, C. A.; Ramos, C.; Zwier, T. S. *J. Am. Chem. Soc.* **1996**, *118*, 4451.
(36) Glicker, S.; Okabe, H. *J. Phys. Chem.* **1987**, *91*, 437.

JP904183A